Structural and Dynamic Characterization of a Vinculin Binding Site in the Talin Rod[†,‡]

Alexandre R. Gingras,[§] Klaus-Peter Vogel,[||] Heinz-Jürgen Steinhoff,[||] Wolfgang H. Ziegler,[⊥] Bipin Patel,[§] Jonas Emsley,[#] David R. Critchley,[§] Gordon C. K. Roberts,*[,§] and Igor L. Barsukov[§]

Department of Biochemistry, University of Leicester, Henry Wellcome Building, P.O. Box 138, Lancaster Road, Leicester LE1 9HN, United Kingdom, FB04-Physik, University of Osnabrück, D-49076 Osnabrück, Germany, IZKF Leipzig, Faculty of Medicine, University of Leipzig, D-04103 Leipzig, Germany, and Centre for Biomolecular Sciences, School of Pharmacy, University of Nottingham, Nottingham NG7 2RD, United Kingdom

Received October 19, 2005; Revised Manuscript Received December 20, 2005

ABSTRACT: Talin is a key protein involved in linking integrins to the actin cytoskeleton. The long flexible talin rod domain contains a number of binding sites for vinculin, a cytoskeletal protein important in stabilizing integrin-mediated cell−matrix junctions. Here we report the solution structure of a talin rod polypeptide (residues 1843−1973) which contains a single vinculin binding site (VBS; residues 1944−1969). Like other talin rod polypeptides, it consists of a helical bundle, in this case a four-helix bundle with a right-handed topology. The residues in the VBS important for vinculin binding were identified by studying the binding of a series of VBS-related peptides to the vinculin Vd1 domain. The key binding determinants are buried in the interior of the helical bundle, suggesting that a substantial structural change in the talin polypeptide is required for vinculin binding. Direct evidence for this was obtained by NMR and EPR spectroscopy. [^{1}H,^{15}N]-HSQC spectra of the talin fragment indicate that vinculin binding caused approximately two-thirds of the protein to adopt a flexible random coil. For EPR spectroscopy, nitroxide spin labels were attached to the talin polypeptide via appropriately located cysteine residues. Measurements of inter-nitroxide distances in doubly spin-labeled protein showed clearly that the helical bundle is disrupted and the mobility of the helices, except for the VBS helix, is markedly increased. Binding of vinculin to talin is thus a clear example of the unusual phenomenon of protein unfolding being required for protein/protein interaction.

Talin (2541 amino acids, ∼270 kDa) is one of a number of cytoskeletal proteins thought to couple the integrin family of cell adhesion molecules to the actin cytoskeleton. The domain structure of talin is entirely consistent with such a role (*1*). The N-terminal globular talin head contains a FERM[1] domain that binds integrins (*2*) [as well as F-actin (*3*)], and recent structural studies reveal how the FERM F3 subdomain interacts with the membrane proximal NPxY motif in the β-integrin subunit cytoplasmic domain (*4*). Interestingly, talin also activates integrins (*5*), probably by relieving the interaction between the α- and β-subunit cytoplasmic domains (*6*). The FERM domain is linked to an elongated flexible rod (*7*) that reportedly contains a second lower affinity integrin binding site (*8*, *9*) and a highly conserved C-terminal actin binding site (*10*, *11*). Talin and the isolated talin rod can both cross-link actin filaments (*12*), consistent with data that suggest that talin is an antiparallel dimer (*13*). Talin also binds several proteins that regulate the dynamic properties of integrin-containing cell−extracellular matrix junctions or focal adhesions (FAs) including FAK (*14*, *15*) and the PIP-kinase type Iγ isoform (*16*−*18*), both of which bind to the FERM domain. PIP2 has been reported to activate the integrin binding sites in talin (*19*), and acidic phospholipids have been shown to bind to the N-terminal region of the protein (*20*). Interestingly, binding of talin to PIP-kinase activates the kinase and results in translocation of the complex to the plasma membrane (*16*). This suggests a model in which the localized production of PIP2 at the membrane activates talin, which in turn binds to and activates integrins, resulting in the assembly of integrin/talin/F-actin complexes that are competent to engage the extracellular matrix.

One of the best characterized talin binding proteins is vinculin (*21*, *22*) which itself has many binding partners including F-actin (*23*−*25*). Biochemical studies show that the binding of talin to vinculin (*26*) (along with binding of most of the other ligands) is inhibited by an intramolecular interaction between the globular vinculin head (Vh) and the C-terminal tail domain (Vt). The recently determined X-ray

[†] This work was funded by grants from the BBSRC (I.L.B. and D.R.C.) and the Wellcome Trust (J.E.) and by DFG Grant STE 640/5 (K.-P.V. and H.-J.S.).

[‡] The coordinates and structural factors for talin 1843−1973 and the VBS3/Vd1 complex have been deposited in the Protein Data Bank as entries 2B0H and 1XWJ, respectively.

* To whom correspondence should be addressed. Telephone: +44 (116) 229-7100. Fax: +44 (116) 229-7053. E-mail: gcr@le.ac.uk.

[§] University of Leicester.

[||] University of Osnabrück.

[⊥] University of Leipzig.

[#] University of Nottingham.

[1] Abbreviations: VBS, vinculin binding site; EPR, electron paramagnetic resonance; FERM, *f*our-point-one, *e*zrin, *r*adixin, *m*oesin; PIP_2, phosphatidylinositol bisphosphate; FAK, focal adhesion kinase; FA, focal adhesion.

10.1021/bi052136l CCC: $33.50
Published on Web 01/20/2006

crystal structure of vinculin provides a molecular basis for these observations (*27*, *28*) and shows that Vt makes extensive contacts with Vh. Although the Vt and talin binding sites in Vh do not overlap, the Vh/Vt interaction is incompatible with the Vh structural changes upon talin binding, thus providing the mechanism for the inhibition of talin/vinculin interaction (*29*). How vinculin is activated within the cell is unclear. PIP2 binds to isolated Vt (*30*, *31*) and has been shown to activate vinculin in vitro (*32*); however, a vinculin mutant deficient in PIP2 binding was able to localize to FAs when expressed in B16 melanoma cells (*33*). The structure shows that the PIP2 binding sites in vinculin are partially masked (*27*), and indeed intact vinculin binds only weakly to PIP2 (*30*). Therefore, the idea has been proposed (*27*) that vinculin is activated by a combinatorial mechanism, which would ensure that vinculin is only activated when two or more binding partners are available. Recruitment of vinculin to FAs can be stimulated by applied force (*34*), raising the possibility that vinculin might be recruited to talin to stabilize the initial weak integrin/talin/F-actin complexes by cross-linking talin to F-actin (*1*). This hypothesis is consistent with the finding that vinculin null cells are still able to assemble FAs, but these are smaller, fewer in number, and more dynamic than in wild-type cells (*33*, *35*−*37*). We originally identified several vinculin binding sites (VBSs) in the talin rod using a series of overlapping talin polypeptides and an SDS blot assay (*38*); three of these (VBS1−3) were further defined using a yeast two-hybrid assay to regions spanning ∼25 amino acids and each corresponding to a single predicted talin amphipathic α-helix (*39*). More recently, we have synthesized all 62 predicted talin rod α-helices (*40*) on filters and have identified an additional eight VBSs (*41*). Moreover, we have used mutant peptides to define the consensus sequence for a VBS as LxxAAxxVAxxVxxLIxxA (*41*). These studies have been complemented by the determination of several structures of complexes of VBS peptides with the D1 domain of the vinculin head (Vd1) (*29*, *41*−*44*) and structures of two adjacent VBS-containing domains from the N-terminal region of the talin rod (*42*, *43*). These show that the hydrophobic residues that define a VBS are themselves "masked" and are buried in the core of a series of helical bundles that make up the talin rod. This implies that the formation of the vinculin/talin complex involves structural changes in both partners, although the kinetic pathway for complex formation remains to be established.

We have now determined the solution structure of talin residues 1843−1973, which contains a single VBS and which is located toward the C-terminal end of the talin rod, near the second integrin binding site and the conserved actin binding site. NMR and EPR spectroscopic studies of the interaction of talin 1843−1973 with the vinculin head show clearly that binding is accompanied by a major structural change in the talin fragment, amounting to unfolding of the helical bundle.

EXPERIMENTAL PROCEDURES

Protein Expression and Purification. The cDNAs encoding murine talin residues 1843−1973, 1843−2008, and 1876−2008 were synthesized by PCR using a mouse talin1 cDNA as template and cloned into the expression vector pET-151/D-TOPO (Invitrogen). Oligonucleotide-directed mutagenesis of talin 1843−1973 was performed using the Invitrogen GeneTailor site-directed mutagenesis system, using the pET-151/D-TOPO plasmid clone as the template for the reactions. The mutants constructed and the nomenclature used for them are given in Table 1. Constructs were expressed in *Escherichia coli* BL21 Star (DE3), cultured either in LB or, for preparation of $^{15}N/^{13}C$-labeled samples for NMR, in minimal media. Recombinant His-tagged talin polypeptides were purified by nickel-affinity chromatography following standard procedures. The His tag was removed by cleavage with AcTEV protease (Invitrogen), and the protein was further purified by anion-exchange chromatography. The recombinant His-tagged chicken vinculin Vd1 domain (residues 1−258) was expressed using a pET-15b expression plasmid and purified as described previously (*43*). The concentration of purified recombinant proteins was determined using the CB-protein assay (Calbiochem).

Table 1: Mutants Constructed for Spin-Labeling Experiments

mutation	position of cysteines in sequence	position of cysteines in structure (Figure 6)	designation
C1953A	1927, 1939	1, 2	SL-C1927/C1939
C1939S, C1953A	1927	2	SL-C1927
N1887C, C1939S, C1953A	1887, 1927	2, 3	SL-C1887/C1927
Q1921C, C1939S, C1953A	1921, 1927	2, 4	SL-C1921/C1927
C1939S, C1953A, R1956C	1927, 1956	2, 5	SL-C1927/C1956

NMR Spectroscopy. NMR experiments for resonance assignment and structure determination of the talin 1843−1973 fragment were performed in buffer comprising 20 mM sodium phosphate, pH 6.5, 50 mM NaCl, and 2 mM DTT. ^2H_2O was added to a final concentration of 10% (v/v) as an internal lock. The protein was concentrated to 1.5 mM using a centrifugal concentrator with a 5 kDa cutoff membrane (Vivascience). For experiments in 100% ^2H_2O, ^{13}C,^{15}N-labeled protein was concentrated to 1.5 mM, flash frozen in liquid nitrogen, lyophilized, and resuspended in the required volume of ^2H_2O. Slowly exchanging H^N protons were deduced from the [^1H,^{15}N]-HSQC spectrum collected immediately after resuspension in ^2H_2O. For titration of talin 1843−1973 with vinculin Vd1, the buffer used was 20 mM sodium phosphate, pH 6.5, 200 mM NaCl, and 5 mM DTT. NMR spectra of talin 1843−1973 were obtained at 30 °C using either a Bruker AVANCE DRX 600 or a Varian INOVA 800 (Biomedical NMR Centre, NIMR, London) spectrometer. Spectra of the talin 1843−1973/Vd1 complex were obtained at 20 °C using an AVANCE DRX 800 equipped with a cryoprobe. All spectra were processed using NMRPipe (*45*) and analyzed with NMRView (*46*). Backbone and side chain assignments were obtained using standard triple- and double-resonance experiments (*47*). The program AUTOASSIGN (*48*) was used for the backbone assignments of talin 1843−1973.

NMR Structure Calculation. Distance restraints were obtained from the following experiments: 4D ^{13}C-edited HMQC-NOESY-HSQC in ^2H_2O (600 MHz, 100 ms), 3D ^{15}N-edited NOESY-HSQC (600 MHz, 100 ms), ^{13}C-edited NOESY-HSQC in H_2O (800 MHz, 100 ms), ^{13}C-edited HMQC-NOESY in ^2H_2O (800 MHz, 100 ms), and 2D

NOESY in ^2H_2O (600 MHz, 100 ms). All NOESY peaks were picked automatically using NMRView, and noise and artifact peaks were removed manually. Cross-peak intensities were used to evaluate target distances. Initial models were generated with CYANA using the CANDID (*49*) method for NOESY cross-peak assignment and calibration. These models were used as initial structures in structure calculation by ARIA (*50*). The acceptance tolerances in the standard protocol of ARIA 1.2 were modified to set violation tolerances to 4.0, 2.0, 1.0, 0.5, 2.0, 1.0, and 0.5 Å for iterations 2−8, respectively, with iteration 1 containing the initial models. Cross-peaks rejected by ARIA were checked manually and, if found reliable, added to the calculation. Two hundred structures were calculated at each iteration, the 20 lowest energy retained and 10 used for final restraint analysis. The 60 lowest energy structures from iteration 8 were further refined in the presence of explicit water molecules. The structural statistics are presented in Supporting Information, Table 1. The set of 20 lowest energy structures has been deposited in the Protein Data Bank (www.rcsb.org) with the accession number 2B0H.

Figures were generated with PYMOL (http://www.pymol.org).

Electron Paramagnetic Resonance Spectroscopy (EPR). After cysteine-substitution mutagenesis the purified proteins were stored in the presence of 2 mM DTT in order to prevent oxidation of the cysteine. Before spin labeling the DTT was removed from the protein solutions by gel filtration using Sephadex G-25 minicolumns from Pharmacia (Uppsala, Sweden). The column was preequilibrated and run in 20 mM sodium phosphate buffer (pH 6.5) and 50 mM NaCl. The protein concentration was adjusted to 20 μM and then incubated with 0.5 mM MTSSL [(1-oxy-2,2,5,5-tetramethylpyrrolinyl-3-methyl)methanethiosulfonate; Toronto Research Chemicals, Toronto, Canada] at 4 °C for 12 h in the dark. The unbound spin label was removed by gel filtration using Sephadex G-25 minicolumns. The spin-label side chain is denoted as SL in the following. For measurements the protein was concentrated using centrifugal concentrators with a 10 kDa cutoff membrane (Vivascience). The final concentration was determined by spin-number calibration of the room temperature spectra using a 0.1 mM MTSSL solution as reference, yielding values from 0.08 mM for SL-C1921/C1927 to 0.64 mM for SL-C1927/C1939, with an average of 0.11 mM over all samples. From this, a labeling efficiency of 0.85 was assumed as verified later; see below. The measurements in the presence of Vd1 were done in excess of the latter by adding an appropriate amount of 0.2 mM Vd1 to the talin 1843−1973 samples. The measured excess of Vd1 was in range of 1.3:1 in case of SL-C1927,1956 up to 2.65:1 in case of SL-C1921/C1927, decreasing the concentration of the labeled protein to about 0.06 mM (between 0.04 mM for SL-C1921/C1927 and 0.08 mM for SL-C1927,1956).

(A) Measurements at Room Temperature. All EPR spectra measured at room temperature (298 K) were recorded using a Varian E-Line 101 X-band cw EPR spectrometer equipped with a H210 rectangular cavity. A modulation frequency of 100 kHz and a modulation amplitude of 1.25×10^{-4} T were used. The applied microwave power was 5 mW. For the spectra of the double mutants where no significant contribution of spin−spin interaction was present, the spectrum of SL-C1927 was subtracted to reveal the spectrum of the second spin-labeled position. Then, to determine the approximate mobility of the spin label at each position, the line width of the central line was determined in the presence and absence of Vd1 by using in-house data analysis routines and compared with published data (*51*).

(B) Measurements at Low Temperature. For measurements of the distance between the two nitroxide electron spins, the samples were cooled to 155 K using an Oxford ESR 9 variable temperature accessory. A homemade cw X-band EPR spectrometer equipped with a Bruker magnet and an AEG H310 rectangular cavity was used. A microwave power of 0.35 mW was applied, and the spectra were recorded using a modulation frequency of 57.5 kHz and a modulation amplitude of 2.3×10^{-4} T. The distance between the two spin labels in the double mutants was determined by fitting calculated spectra to the measured data (*52*). For the *g*-tensor fixed values of $g_{xx} = 2.0085$, $g_{yy} = 2.0066$, and $g_{zz} = 2.0029$ were used. The A_{xx} and A_{yy} components of the hyperfine tensor *A* were also kept fixed at 6.1 and 4.7 G, respectively. The A_{zz} component was treated as a variable in the fitting as it is very sensitive to the polarity of the spin-label environment. The calculated stick spectrum was convoluted with a field-independent line-shape function, composed of a superposition of 45% Gaussian and 55% Lorentzian lines with line widths of 3.85 and 2.88 G, respectively, as derived from the analysis of SL-C1927. In fitting the spectra of the double mutants which show a dipolar broadening, a second, nonbroadened component was included to represent a certain fraction of singly labeled proteins. This unbroadened fraction amounts to (11 ± 5)% of the total signal, which agrees reasonably with the estimated labeling efficiency of 85%.

Vinculin Head Binding to a Peptide Array. Talin VBS peptides (25-mers) based on the mouse talin VBS3 sequence were SPOT-synthesized on a cellulose membrane (*53*) with 0.5 nmol of peptide per spot. Membranes were blocked overnight in Tris-buffered saline (TBS, 50 mM Tris-HCl, pH 7.0) with 10% fetal bovine serum. Glutathione *S*-transferase (GST) tagged mouse vinculin Vd1 (1−258) was expressed using pGEX-4T (Amersham Biosciences) and purified as described previously (*33*). Membranes were overlaid for 2 h with GST-Vd1 (50 nM) in TBS with 1% BSA. Bound GST-Vd1 was detected using a polyclonal GST antibody (Sigma) and alkaline phosphatase (AP) coupled anti-rabbit Ig (Sigma) as described previously (*43*). In the SPOT-peptide assay, Cys1953 was ACM (*S*-acetamidomethyl) protected to prevent oxidation. Since unprotected Cys could not be used in the assay, Ala, Ser, and 2-aminobutyric acid were tested instead, and all three provided a stronger signal than VBS3 with ACM-Cys (Supporting Information, Figure 1). Hence the use of ACM-Cys resulted in a generally reduced affinity of talin VBS3 for Vd1. In chicken talin position 1953 is occupied by Ser, and chicken VBS3 revealed the highest affinity for Vd1 as compared to VBS1 and VBS2 by surface plasmon resonance (*44*).

Proteolysis. All proteolysis experiments were carried out using a 1:20 (w/w) trypsin:protein ratio and incubated at 20 °C for 1 h.

Gel Filtration. Analytical gel filtration chromatography of recombinant talin 1843−1973 and vinculin Vd1 (1−258) was performed using Superdex-75 (10/30) (Pharmacia) at room temperature. The column was preequilibrated and run

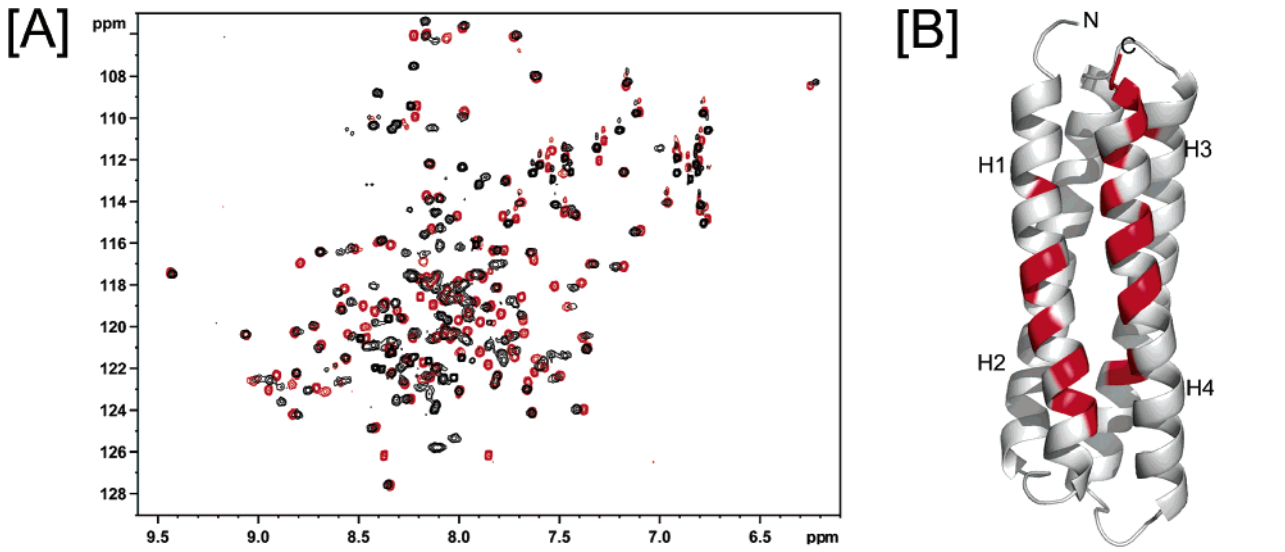

FIGURE 1: Characterization of the talin polypeptides containing VBS3. (A) Superposition of the 2D [^{1}H,^{15}N]-HSQC spectra of talin 1843−1973 (red) and talin 1843−2008 (black). (B) Effect of the C-terminal helix extension on the amide chemical shifts in talin 1843−1973. The residues highlighted in red show significant chemical shift changes (>0.05 ppm in the ^{1}H dimension).

in 20 mM Tris-HCl, pH 8.0, 200 mM NaCl, and 2 mM DTT at a flow rate of 0.8 mL/min. In each case, 0.5 mL fractions were collected and analyzed using a 15% SDS−PAGE gel and stained using the GelCode blue reagent (Pierce).

RESULTS

Mapping of the VBS3 Boundaries. To clarify the domain structure in the region of talin containing VBS3 (residues 1944−1969), we began with secondary structure predictions on the whole talin rod (*41*) and structural information on the VBS1 five-helix bundle (*43*) and the VBS2 four-helix bundle (*42*). One of the common features of the VBS1 and VBS2 structures is that in both cases the VBS α-helix is the fourth helix in the bundle. We thus cloned three new talin polypeptides: 1843−2008, predicted to contain five helices, 1843−1973 (four helices), and 1876−2008 (four helices). The expression level of the talin 1876−2008 construct was very low, suggesting that the protein does not fold properly, whereas talin 1843−2008 expressed well. However, limited proteolysis followed by N-terminal sequencing and mass spectroscopy showed that talin 1843−2008 is readily cleaved by trypsin at R1973 (data not shown) to yield a talin 1843−1973 polypeptide. Indeed, talin 1843−1973 was resistant to both chymotrypsin and trypsin treatment.

The 1843−2008 and 1843−1973 fragments were also characterized by comparing 2D [^{1}H,^{15}N]-HSQC spectra of the uniformly ^{15}N-labeled proteins. The spectrum of talin 1843−1973 (four-helix) shows a good dispersion of the signals with few sharp peaks, indicative of a well-folded protein (Figure 1A, red spectrum). The spectrum of talin 1843−2008 (Figure 1A, black spectrum) shows a very similar pattern of chemical shifts, indicating that the fold of the four-helix construct is conserved after the addition of an extra helix at the C-terminus, but it has, in addition, a number of broader cross-peaks and a small number of sharp peaks close to the middle of the ^{1}H^N region. This suggests that the C-terminal extension has a more dynamic structure than the rest of the protein and is likely to be loosely attached to the folded protein core. This is consistent with the proteolysis data, indicating that the stable structured domain in this region of the talin rod comprises residues 1843−1973, making this the choice for NMR structure determination.

NMR Structure of the Talin 1843−1973 Fragment. Talin 1843−1973 in solution gives a well-resolved NMR spectrum, with line widths corresponding to a monomeric state. The resonances have been assigned by conventional triple-resonance experiments using ^{13}C,^{15}N-labeled protein, and the solution structure has been determined using 3731 unique and 725 ambiguous distance constraints from NOEs and 218 TALOS dihedral angle constraints from ^{13}C chemical shift values (Supporting Information, Table 1). The N-terminal (1843−1849) and the C-terminal (1971−1973) residues are unstructured and flexible, as indicated by the relatively weak intraresidue and sequential NOEs, absence of medium- and long-range NOEs, and narrow lines observed for these regions. The core of the fragment, residues 1850−1970, forms an up−down−up−down four-helix bundle (Figure 2A,B) with the helices connected in a right-handed topology. All four helices in the bundle are α-helices, well characterized by an extensive set of H^N_i/H^α_{i-3}, H^N_i/H^α_{i-4}, and H^β_i/H^α_{i-3} NOEs. Helices H1, H2, and H4 have similar lengths of ∼25 residues, while helix H3 is slightly longer (∼29 residues). The helices are mostly straight, except for helix H3, which has a kink in the middle, corresponding to the region Gly1924−Gly1926 highlighted in blue in Figure 2B. The signal of the NH group of Gly1926 is not observed in any of the spectra recorded, most likely due to exchange broadening, consistent with a break in the helix in this region. Helix H2 contains a proline residue at both the N- and C-termini (Pro1884 and Pro1902) which introduce slight kinks at each end of the helix. The helices are nearly antiparallel, with a larger angle between the helix pairs H1 + H4 and H2 + H3. All of the helices are connected by short tight loops which are well defined, as seen in Figure 2A.

All four helices of talin 1843−1973 are amphipathic, with their more hydrophobic surfaces buried in the interior of the bundle. This is represented in Figure 2B where the hydrophobic residues have been color coded in green. At the end of the bundle where the N- and C-termini of the fragment

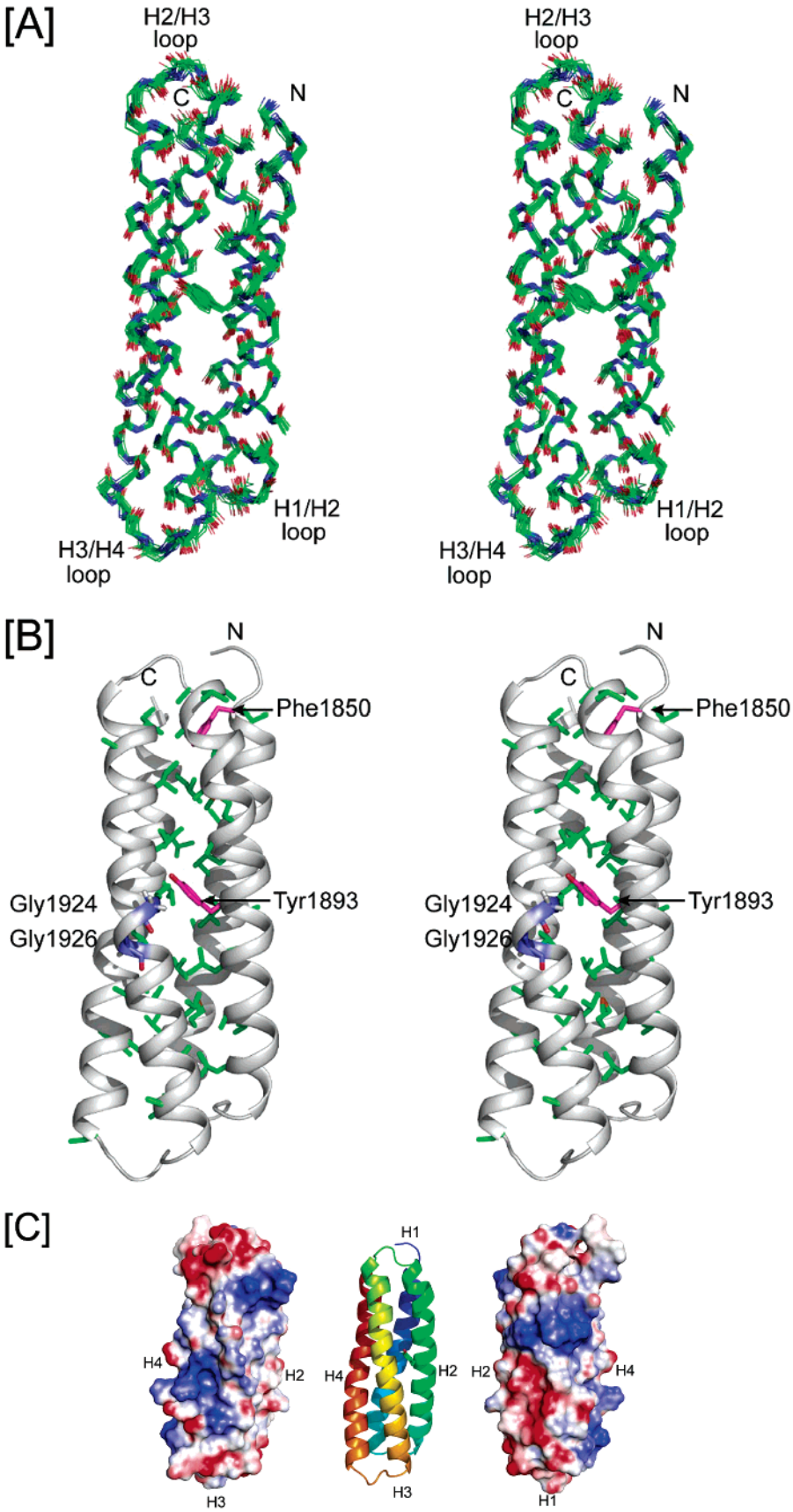

FIGURE 2: Solution structure of talin 1843−1973. (A) Stereoview of the superposition (using backbone atoms) of the 20 lowest energy structures consistent with the NMR data. Only the structural core region (residues 1850−1970) is shown, not the disordered N- and C-termini. The side chain of Tyr1893 is included to show that it is well defined. (B) Stereoview of a representative low-energy structure (only residues 1847−1973) showing the hydrophobic residues comprising the hydrophobic core in green. Also highlighted are Tyr1893 and Phe1850 in magenta and Gly1924 and Gly1926 in blue. (C) Ribbon diagram of talin 1843−1973 (center) with helices labeled H1−H4 from the N-terminus. A molecular surface representation of the same orientation as the ribbon diagram is shown at the left and the opposing view 180° rotated at far right, with positively charged surface regions in blue and negatively charged regions in red.

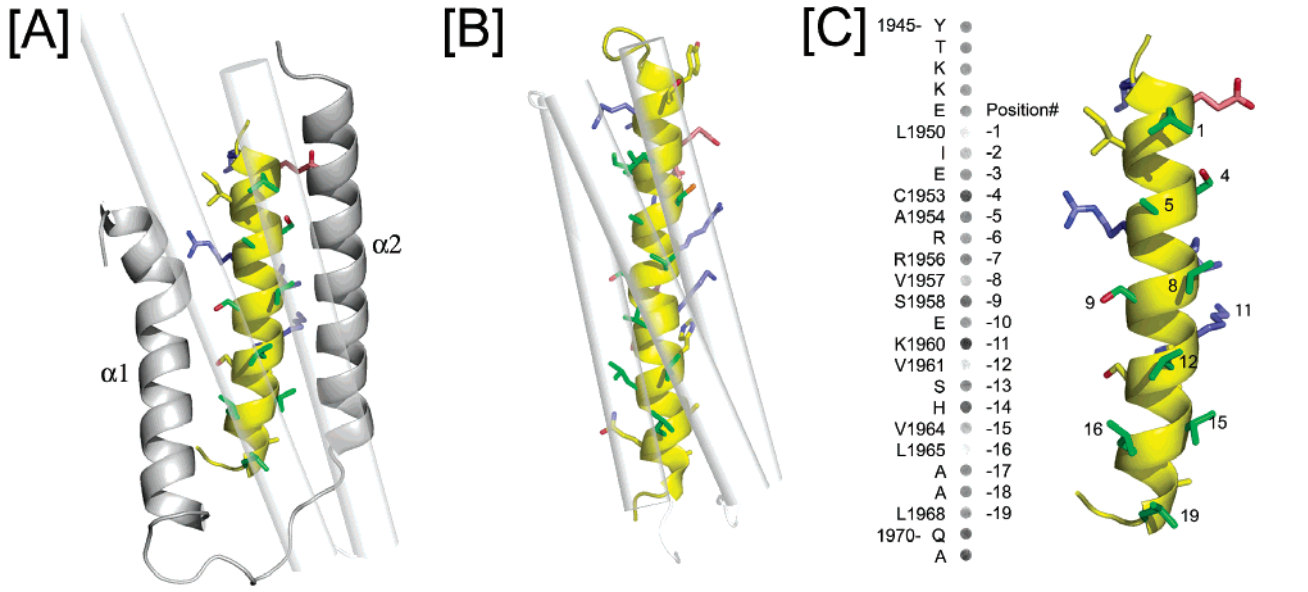

FIGURE 3: Basis of the talin VBS3 helix binding to vinculin Vd1. (A, B) Comparison of the location of the vinculin binding residues of VBS3 (H4) in (A) the complex with Vd1 and in (B) free talin 1843−1973. (C) Analysis of Vd1 binding to a series of 25 VBS3 synthetic peptides (26-mers) in which each residue in turn was substituted by alanine. The peptides were SPOT-synthesized on a cellulose membrane, and bound Vd1 was detected using a polyclonal GST antibody. The VBS3 sequence is shown vertically on the left with each spot shown for the respective peptide containing alanine substitution. The talin VBS3 (H4) helix is shown as a yellow ribbon, in the same orientation in all cases; basic residues are highlighted in blue, acidic in red, highly buried (>75%) in green, and all others in yellow.

are located, the hydrophobic core is capped by the aromatic ring of Phe1850 (highlighted in magenta in Figure 2B) which makes extensive contacts within the hydrophobic core and is protected from the solvent. The aromatic ring of Tyr1893 (highlighted in magenta in Figure 2B) in helix H2 lies almost perpendicular to the hydrophobic core between helices H2 and H3, with its hydroxyl group and one edge of the aromatic ring exposed to the solvent. Just opposite Tyr1893, on helix H3, Gly1924 creates extra room for the aromatic ring to slide inside the core of the bundle. The position of the tyrosine aromatic ring is well defined due to the large number of observed long-range NOEs that involve aromatic ring protons. In the C-terminal half of helix H2 several alanine residues form a continuous surface that makes contact with the internal hydrophobic cluster. Due to the small and uniform size of these hydrophobic side chains such a surface is less optimal for maintaining the integrity of the hydrophobic core than surfaces composed of larger hydrophobic residues. In combination with the proline-induced kinks at both ends of the helix and the glycine residues in the neighboring helix H3, the alanine clustering is expected to reduce the stability of the structure in the region. This was confirmed by the fast H/D exchange rate observed for all of the amide protons of helix H3. By contrast, helices H1 and H4 contain a large number of hydrophobic residues making an extensive set of interhelical contacts. The H/D amide exchange rate showed that the most slowly exchangeable protons are predominantly located in the C-terminal part of the helix H1 and the residues from other helices that make contacts with this part of the helix H1. This suggests the formation of a particularly stable hydrophobic cluster in the part of the bundle that is distant from the N- and C-termini.

Defining the Location of the C-Terminal Extension to the Talin 1843−1973 Fragment. The surface of the talin 1843−1973 bundle is made up predominantly of charged or polar residues (Figure 2C). However, there is a relatively large flat hydrophobic patch in the vicinity of Tyr1893 between helices H2 and H3, and there is a narrow groove of hydrophobic and polar side chains between helices H1 and H4. These hydrophobic regions may be important for the assembly of successive helical bundles in the talin rod structure, and this was explored by compring talin 1843−1973 and talin 1843−2008.

The differences in chemical shifts in the 2D [^{1}H,^{15}N]-HSQC spectra between talin 1843−1973 and talin 1843−2008 indicate the contact surface for the C-terminal 35-residue extension which, according to the secondary structure prediction, corresponds to an additional helix. Most of the chemical shifts for the well-resolved peaks remain unchanged. Using the resonance assignment of talin 1843−1973, we mapped all of the significant chemical shift changes (>0.05 ppm in the ^{1}H dimension) in the talin 1843−2008 spectra onto the structure of the four-helix bundle. The majority of the changes (shown in red in Figure 1B) cluster on the part of the surface of the bundle made up by helices H1 and H4. As noted above, this surface region contains a narrow hydrophobic groove between helices H1 and H4, flanked by charged and polar residues (Figure 2C). The presence of broad cross-peaks in the HSQC spectrum of fragment 1843−2008 suggests a transient interaction between the core four-helix bundle of the smaller fragment and the additional C-terminal helix in talin 1843−2008. This is supported by the results of trypsin proteolysis, which showed that talin 1843−2008 was cleaved after Arg1973 to release a fragment identical to 1843−1973.

The Key Determinants of Talin VBS3 Binding to Vd1. Talin VBS3 was originally mapped using a yeast two-hybrid assay (*39*) to residues 1944−1969 (VBS3) and encompasses the length of helix H4 of the talin 1843−1973 four-helix bundle. The structures of several complexes between peptides corresponding to talin VBSs and Vd1 (*41*−*44*), including the VBS3/Vd1 structure (*29*), have been reported recently and are all very similar to one another. (We have also determined the structure of the VBS3/Vd1 complex, and this

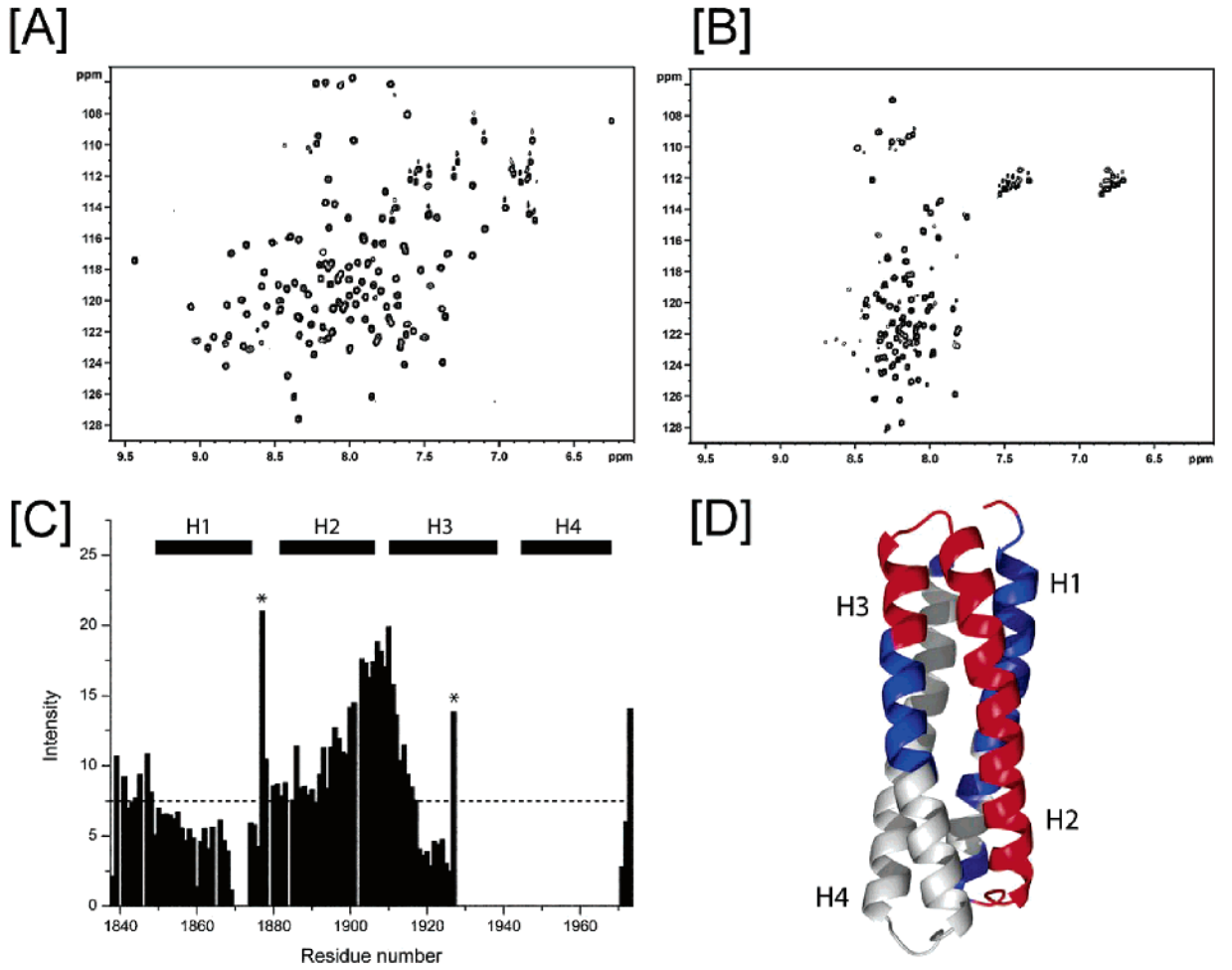

FIGURE 4: NMR analysis of the interaction between talin 1843−1973 and Vd1. (A, B) Two-dimensional [^{1}H,^{15}N]-HSQC spectra of uniformly ^{15}N-labeled talin 1843−1973: (A) free protein and (B) the gel filtration-purified talin 1843−1973/Vd1 complex. (C) Intensities (arbitrary units) of the cross-peaks in the [^{1}H,^{15}N]-HSQC spectrum of ^{15}N-labeled talin 1843−1973 bound Vd1 as a function of sequence position. The position of the helices in free talin 1843−1973 are indicated by the black bars, and the asterisks (*) indicate overlapped cross-peaks. A dotted line was traced at intensity 7.5 as a chosen reference point for the color coding shown in panel D. (D) Mapping of the cross-peak intensities of vinculin-bound talin 1843−1973 on the structure. The talin 1843−1973 residues with high-intensity cross-peaks (>7.5) in the complex are color coded in red, those with low intensity in blue (<7.5), and the residues that could not be assigned in white.

structure has been deposited in the Protein Data Bank with the accession number 1XWJ.) The contacts made between the talin VBS3 helix and Vd1 (Figure 3A) are compared to those made by VBS3 within the talin four-helix bundle (residues 1843−1973) in Figure 3B; this comparison shows clearly that the hydrophobic face of the amphipathic talin VBS3 helix is buried within the Vd1 complex just as it is within the four-helix bundle of talin 1843−1973. It is thus clear that binding of the talin VBS3 to Vd1 can only take place if the talin four-helix bundle structure undergoes a major conformational change.

To define the basis of the specificity of the VBS3/Vd1 interaction, we synthesized a series of 25 peptides, each containing a single alanine substitution in the native VBS3 sequence. This array was prepared by SPOT synthesis (*53*) on a cellulose membrane and assayed for effects on Vd1 binding using an ELISA-type procedure. The results are mapped onto the structure of the VBS3 peptide in Figure 3C. Substitution of Leu1950, Val1957, Val1961, Val1964, or Leu1965 on the buried face of the talin VBS3 helix (helix 4) all resulted in reduced binding. However, an increase in binding is observed on substitution of Cys1953 and Lys1960. The data indicate that key hydrophobic residues on the buried face of the VBS3 helix form the principal contacts with Vd1.

Talin VBS3 conforms to the consensus VBS sequence determined previously (*41*) and does not show any "rule violations". VBS3 has a Lys in position 11 which is conserved as a small residue (either Ala or Ser) in all other talin VBS helices. However, position 11 was shown to be the most relaxed of the buried positions, allowing charged residues such as Lys and Arg, and only excluding Trp, Asp, Gly, and Pro. In the VBS3/Vd1 complex structure, the Lys1960 side chain in position 11 is bent toward the outside of Vd1 and hydrogen bonds to the Lys1956 in position 7. As predicted, substitution of the Lys in position 11 to Ala increases Vd1 binding as shown by SPOT-peptide analysis (Figure 3C).

NMR Characterization of the Talin 1843−1973/Vinculin Vd1 Interaction. The formation of a complex between talin 1843−1973 and vinculin Vd1 was monitored by [^{1}H,^{15}N]-HSQC NMR (Figure 4). On addition of unlabeled Vd1 to ^{15}N-labeled talin 1843−1973, the cross-peaks in the spectra corresponding to the free talin domain decreased in intensity and disappeared when the Vd1:talin ratio was >1. At the

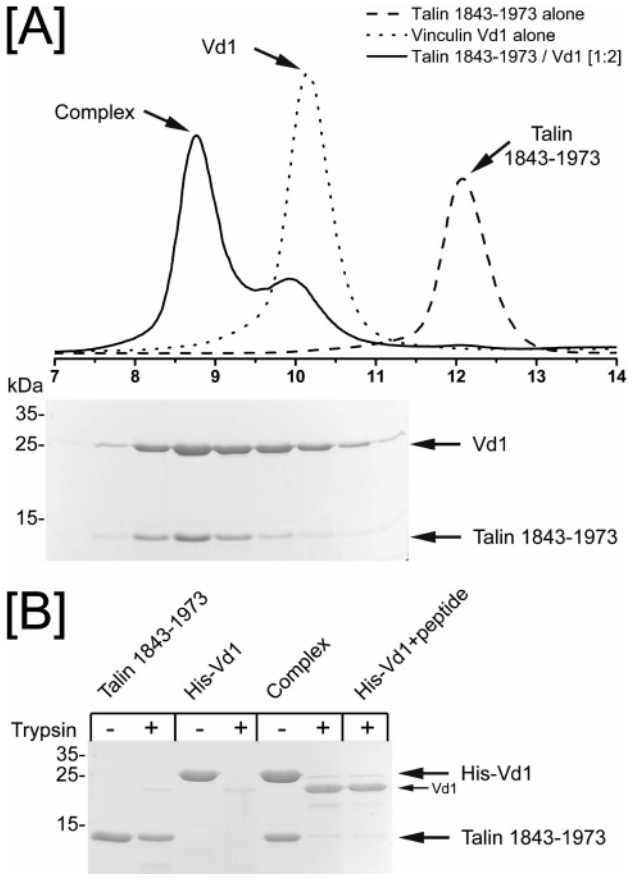

FIGURE 5: Characterization of the talin 1843−1973 interaction with vinculin Vd1 by gel filtration and proteolysis. (A) Superdex-75 (10/30) gel filtration chromatography of talin 1843−1973 in the presence or absence of the vinculin Vd1 domain. Fractions were collected and analyzed using SDS−PAGE. At a 1:2 molar ratio of talin 1843−1973/Vd1 (solid line), all of the talin is in complex with the Vd1, and some free Vd1 is detected; this indicates a high-affinity interaction. (B) Limited proteolysis of talin 1843−1973 and vinculin Vd1. Free talin 1843−1973 is resistant to trypsin treatment, while free Vd1 is sensitive to proteolysis and is degraded by trypsin. When Vd1 is incubated with talin 1843−1973 or a synthetic VBS3 peptide, Vd1 becomes partly protease resistant, while talin 1843−1973 becomes protease-sensitive in the complex.

same time, a new set of cross-peaks arising from talin 1843−1973 in complex with Vd1 appear in the spectra and increase in intensity with increasing Vd1 concentration. Quantitative titrations showed that complete disappearance of the resonances of free talin 1843−1973 required addition of approximately equimolar Vd1. The formation of a 1:1 talin/vinculin complex was confirmed by analytical gel filtration (Figure 5A).

A comparison of the spectra of talin 1843−1973 in the free form and in complex with Vd1 is shown in panels A and B of Figure 4; the characteristics of the [^{1}H,^{15}N]-HSQC spectrum of the complex are clearly very different from those of the corresponding spectrum of the free form. In the spectrum of the complex (Figure 4B), only 83 cross-peaks are observed, approximately two-thirds of the number observed for the free protein (Figure 4A). The cross-peaks in the spectrum of the complex can be divided into three groups: a group of relatively sharp intense cross-peaks, a group of substantially broader, but still intense peaks, and finally a number of much weaker broad peaks. In all cases, the chemical shift dispersion is much less than for the free protein. The decreased number of cross-peaks observed in this spectrum provides evidence for highly heterogeneous motional properties of the talin fragment in the complex, and the narrow line widths and limited chemical shift dispersion of those cross-peaks which are observed suggest that they arise from highly mobile and predominantly unstructured regions of talin 1843−1973. The resonances of talin 1843−1973 in the complex were assigned using a standard set of triple-resonance experiments. The intensities of the observed cross-peaks are plotted against the sequence in Figure 4C and indicated on the structure in Figure 4D. The cross-peaks which are not observed in the complex map onto helix H4, the VBS3 that makes a direct contact with vinculin, the C-terminal half of helix H3, and a short stretch in the C-terminal region of helix H1. The highest cross-peak intensities correspond to helix H2 and the N-terminal part of helix H3.

The stability of the proteins in the complex was assessed by a limited proteolysis experiment. Figure 5B shows that, in the presence of trypsin, talin 1843−1973 is stable whereas vinculin Vd1 is sensitive to proteolysis. Formation of the talin 1843−1973/vinculin Vd1 complex results in a stabilization of Vd1 to proteolysis, while talin 1843−1973 becomes sensitive to proteolysis, consistent with the substantial unfolding of the talin helical bundle suggested by the HSQC spectra. Incubation of vinculin Vd1 with a synthetic VBS3 peptide also resulted in a stable complex in which Vd1 was resistant to proteolysis. These data indicate that in isolation vinculin Vd1 has a conformationally dynamic fold whereas, upon binding to talin, a structurally stable complex is formed between Vd1 and residues spanning the VBS3 helix from talin.

EPR Characterization of the Talin 1843−1973/Vinculin Vd1 Interaction. To obtain further information on the effects of vinculin Vd1 binding on the mobility and structure of the talin four-helix bundle, we have used the site-directed spin-labeling approach (*54*, *55*). Five different mutants of talin 1843−1973, listed in Table 1, were designed to place cysteine residues at key positions on the four-helix bundle, selected to probe interhelical contacts and the integrity of helix H3, as shown in Figure 6A. These mutants have been labeled with a nitroxide spin label, MTSSL, to give singly or doubly spin-labeled proteins, the EPR spectra of which then provide information on the local mobility and on the distances between the nitroxides, both in the free protein and in its complex with Vd1.

(A) Mobility Measurements. The line width of the central line of the spectrum of each labeled mutant gives a measure of the mobility of the spin label; this has been shown to correlate with the local structure at the site of labeling (*51*). SL-C1927 was labeled at a single position in helix H3 of the four-helix bundle as shown in Figure 6A. Figure 6B shows the spectra obtained from this spin-labeled mutant in the absence and presence of vinculin Vd1. In the absence of Vd1 two components of the high-field line are visible in the spectrum, indicating a restricted motion of the nitroxide arising from a tertiary interaction. This is consistent with the NMR structure, which shows C1927 pointing toward helix H2. In the presence of Vd1 the spectral component which represents the restricted motion vanishes and the spectrum as a whole becomes sharper; the changes in inverse line width of the central line are presented in Table 2. The

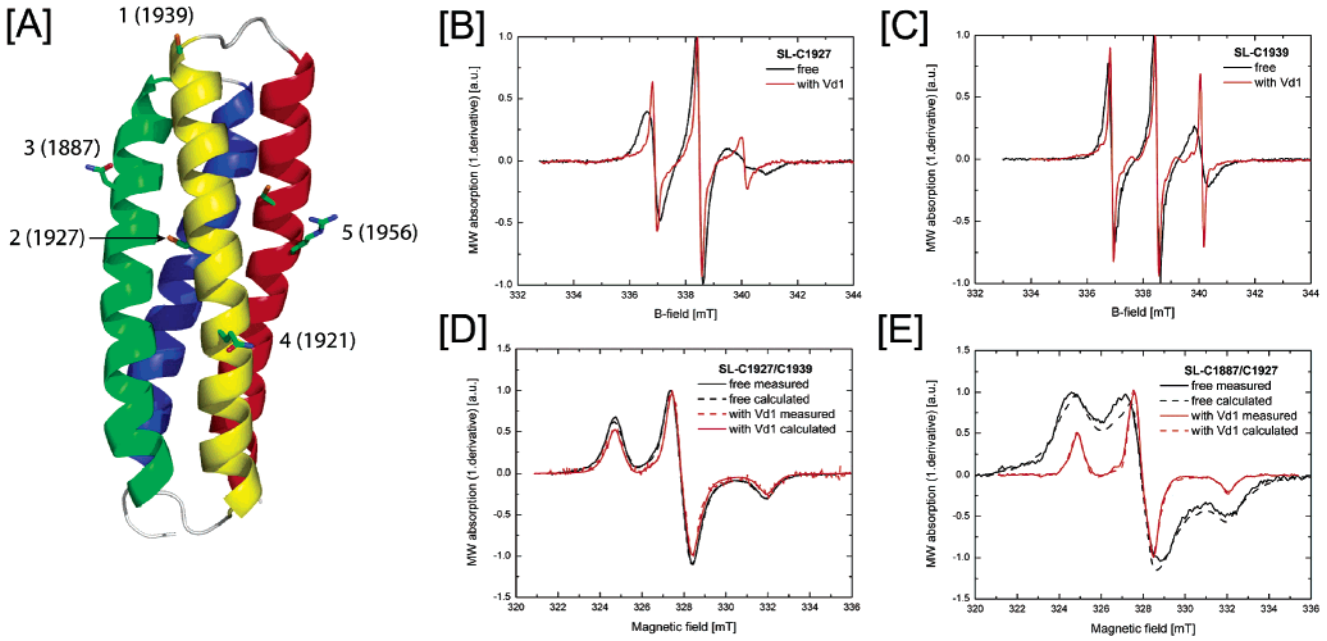

FIGURE 6: EPR spectroscopy of spin-labeled talin 1843−1973. (A) Structure of talin 1843−1973 showing the selected positions for spin labeling. (B) Room temperature (298 K) cw EPR spectra of SL-C1927. In the absence of Vd1 (black line) the line shape indicates a moderately mobile spin label with signs of tertiary interaction visible for this region. After addition of Vd1 the mobility increases (red line), showing a line shape corresponding to a opened, disordered structure. (C) Room temperature (298 K) cw EPR spectra of the spin label at position 1939, obtained by subtracting the corresponding spectra of SL-C1927 from those of SL-C1927/C1939. The initial mobility of the spin-labeled side chain (black line) is higher than that of position 1927. In the presence of Vd1 (red line) the major component exhibits a decreased line width, reflecting increased mobility; in addition, a minor component with a plateau around 336 mT appears, representing a tertiary interaction, probably with Vd1. (D) Measured (solid) and calculated (dashed) low-temperature (155 K) cw X-band EPR spectra of SL-C1927/C1939 in the absence (black) and presence (red) of Vd1. The theoretical spectra were calculated using a Gaussian distance distribution of 4.0 Å and mean distance of 14.9 Å in the first and 17.2 Å in the second case. (E) Measured (solid) and calculated (dashed) low-temperature (155 K) cw X-band EPR spectra of SL-C1887/C1927 in the absence (black) and presence (red) of Vd1. The theoretical spectra were calculated using a Gaussian distance distribution of 4.0 Å and mean distance of <9 Å in the first and >20 Å in the second case, indicating a dramatic increase of the interspin distance between the two labeled positions on binding to Vd1.

Table 2: Local Structure Close to the Spin-Labeled Positions Inferred (According to Ref *51*) from Spin-Label Dynamics Indicated by EPR Line Width Determination

position	Vd1	inverse line width,[a] G^{-1}	local structure
SL-C1887	−	NA	NA
	+	$0.88^{+0.19}_{-0.13}$	loose random coil
SL-C1921	−	NA	NA
	+	$0.74^{+0.13}_{-0.10}$	loose random coil
SL-C1927	−	$0.39^{+0.03}_{-0.03}$	helical suface/loop
	+	$0.60^{+0.08}_{-0.06}$	loose random coil
SL-C1939	−	$0.41^{+0.04}_{-0.03}$	helical suface/loop
	+	$0.71^{+0.12}_{-0.08}$	loose random coil
SL-C1956	−	$0.20^{+0.01}_{-0.01}$	interaction with tertiary structure[b]
	+	NA	*c*

[a] Inverse line width of the mid-field line from room temperatrure (298 K) cw X-band EPR measurements. [b] Line width likely overestimated due to the close distance between SL-1927 and SL-1956. [c] Only the mobile component is accessible, but the distance between the low- and high-field peaks indicates an interaction with the tertiary structure.

spectrum of the complex indicates a very high mobility of the nitroxide in SL-C1927, suggesting that, in the complex, helix H3 has become disordered and that the spin label is no longer close to helix H2.

To obtain comparable information about the doubly labeled samples, all of which have a spin label on C1927, it is necessary to subtract the spectrum of SL-C1927; this can only be done where there is no spin−spin interaction between the two nitroxides. The results of this subtraction for SL-C1927/C1939 are presented in Figure 6C and show that the mobility of the nitroxide at C1939 also increases on addition of Vd1, to that characteristic of a loose random coil. A very small second, immobile, component appears in the spectrum of the complex around 335.5 and 343 mT, representing an interaction of the nitroxide with the tertiary structure, probably with Vd1. For SL-C1887/C1927 and SL-C1921/C1927, the two spin labels are sufficiently close in space (see below) to lead to strong spin−spin interaction in the absence of Vd1, and therefore no information can be obtained concerning the mobility of the nitroxides attached to C1887 or C1921. However, after adding Vd1, this spin−spin interaction disappears, revealing a very high mobility for the spin labels at positions 1887 and 1921. This indicates that the corresponding parts of helix H2 and helix H3 have become disordered on formation of the complex. Finally, for SL-C1927/C1956, the extracted spectrum of the nitroxide attached to C1956 (located in the middle of the VBS helix, Figure 6A) shows a nitroxide which is more immobile than that attached to C1927, indicating that the VBS helix H4 is probably more rigid than helix H3. (The line width of ∼5 G may be somewhat overestimated as there are signs of line broadening due to spin−spin interaction in this sample.) In the presence of Vd1, SL-C1927/C1956 gives a composite spectrum of two components, where one is more mobile and one less mobile than in the absence of Vd1. Spin number calculation shows that the immobile component contributes

Table 3: Results of Distance Measurements on Doubly Spin-Labeled Talin 1843−1973 and Comparison with NMR Results

distance between	Vd1	singly labeled fraction (±0.05)	distance[a] between nitroxide groups, Å	distance[a] in structure of free protein, Cβ−Cβ, Å
SL-C1927, SL-C1939	−	0.12	14.85 ± 0.20	18.53
	+	0.15	17.20 ± 0.20	
SL-C1887, SL-C1927	−	0.06	<9	10.77
	+	NA	>20	
SL-C1921, SL-C1927	−	0.10	11.0 ± 0.50	10.61
	+	0.10	16.50 ± 0.20	
SL-C1927, SL-C1956	−	0.10	14.50 ± 0.20	10.80
	+	NA	>20	

[a] Note that the distances derived from EPR are those between the nitroxide groups at the end of the spin-label side chains, while in the case of the solution structure of the free protein the distance was measured between the Cβ atoms of the corresponding residues.

more than ~90% to the spectral intensity, indicating that the nitroxide at position 1956 is predominantly interacting with tertiary structure elements, most likely with Vd1.

(B) Distance Measurements. EPR measurements at low temperature were carried out to determine the distances between the two nitroxide groups within each of the doubly labeled mutants, using the effects on line width and shape of the spectrum arising from the dipolar interaction between the unpaired electrons of the two nitroxide side chains. The derived distances between the NO groups of each pair of spin labels are given in Table 3 and compared to the Cβ−Cβ distances between the corresponding side chains from the NMR structure. The measured interspin distance of 11 Å for SL-C1921/C1927 is very close to the Cβ−Cβ distance of 10.61 Å in the NMR structure and is also in agreement with an α-helical structure in this region. The distance increases by 5.5 (±1.0) Å after adding Vd1 to the sample. Since the labeled positions, 1921 and 1927, are only six residues apart, a distance of 16.5 Å in the presence of Vd1, taken together with the high mobility of the nitroxide, is incompatible with an α-helical structure in the complex. For SL-C1927/C1939 (Figure 6D) the distance between the two spin labels increases only slightly, by 2.4 (±0.4) Å, on addition of Vd1. This would still be consistent with an α-helical structure in this region in the complex; however, the mobility estimated for the nitroxide on C1939 rules out the existence of a stable helix. In both SL-C1887/C1927 (Figure 6E) and SL-C1927/C1956 the spin labels are on different helices, and in both cases the clear spin−spin interaction observed in the isolated talin 1843−1973 is consistent with the four-helix bundle structure. However, neither of these samples shows any spin−spin interaction in the complex with Vd1, indicative of an inter-nitroxide distance of >20Å, of a substantial separation of helices H2 and H3 and H3 and H4, and hence of the unfolding of the four-helix bundle on complex formation.

DISCUSSION

Sequence analysis predicts the formation of amphipathic helices all along the talin rod (*40*), but the high sequence similarity within the helices makes it impossible to predict any domain structure. The existence of domains within the rod is, however, suggested by electron microscopy (*7*), limited proteolysis, and our previous structural studies (*42*, *43*). The identification in the present work of a stable folded domain in the middle of the talin rod provides further evidence that helical bundles are the smallest structural units of the talin rod. These basic helical bundle units are likely to be organized into higher order structures in the talin rod, either through the expansion of the helical bundle, as suggested by our model of the 656−889 fragment (*42*), or in a staggered arrangement, as in the 482−789 fragment (*43*).

The VBS3-containing fragment 1843−1973 forms a four-helix bundle, in line with the secondary structure prediction of four amphipathic helices. Interestingly, the bundle has a right-handed topology, in contrast to the left-handed topology of the N-terminal talin domains (*42*, *43*), perhaps reflecting the packing requirements in the whole talin rod. The 1843−1973 fragment has two charged faces on opposite sides of the molecule, one flat relatively hydrophobic surface stretching along the whole length of the bundle between helices H2 and H3 and a smaller hydrophobic patch on the opposite face, between helices H1 and H4. These surfaces are possible sites of interaction with the adjacent talin domains. Indeed, the chemical shift differences between the four-helix 1843−1973 and five-helix 1843−2008 talin polypeptides suggest that the next domain in the C-terminal direction interacts with the area between helices H1 and H4. This would leave the large hydrophobic surface between helices H2 and H3 as the site of the interaction with the next domain in the N-terminal direction. The larger hydrophobic surface of the VBS3-containing domain resembles that of the VBS2-containing fragment (*42*). In the latter case, where structural information is available on a neighboring fragment, we have suggested that additional N-terminal helices would expand the helical bundle through the nearly parallel packing of the helices. A similar arrangement is expected at the N-terminus of the VBS3-containing domain, with the packing of the additional helices decreasing the exposed hydrophobic surface area.

The general features of the interaction between the 1843−1973 helical bundle and vinculin follow a pattern similar to those reported earlier for the VBS2-containing bundle (*42*), although the picture for talin 1843−1973 is simpler since, as indicated by gel filtration and NMR, it binds Vd1 with 1:1 stoichiometry. In the complex most of the talin domain is disordered and highly mobile, apart from the VBS which becomes embedded into the vinculin structure. Clear evidence for this dramatic unfolding comes from NMR and EPR spectroscopy. In the present case, the information from the HSQC NMR spectra of this 43 kDa complex is restricted to the unstructured regions that are sufficiently mobile for their resonances to be observed and assigned. The observation of such sharp signals with limited chemical shift dispersion demonstrates local unfolding of the structure. The resonances from residues which are either in direct contact with vinculin or in adjacent parts of the structure are broadened too much to be observable in these spectra. The exact mechanism of the talin unfolding upon complex formation is currently unclear. The talin helical fold is stable as evidenced by the proteolysis experiments, suggesting an active role of the initial vinculin/talin contact in the unfolding process. This unfolding is likely to be facilitated by the existence of regions of decreased local stability in the talin structure (see below).

To obtain additional information on the structural and dynamical properties of the talin fragment in the complex, we introduced nitroxide spin-label pairs, positioned so as to probe interhelical contacts and the integrity of helix H3. The derived interspin distances on the free protein are in good agreement with the proposed four-helix bundle structure, and the mobility data show for position 1927 (on the surface of helix H3) a line width which, according to the correlation of McHaourab et al. (*51*), suggests a position on the surface of a helix, with some tertiary interaction, most likely with helix H2. Similarly, the higher mobility for the spin label at position 1939 corresponds well with its position in the structure, at the tip of helix H3. The addition of vinculin Vd1 results in a clear increase in the mobility of the nitroxides in all positions apart from that at position 1956 in the VBS, and the interhelical distances increase dramatically, lending strong support to the proposal that the helical bundle structure unfolds completely on binding Vd1. Within helix H3, a large increase in the inter-nitroxide distance is observed for positions 1921−1927 in the N-terminal half of the helix H3, while a smaller distance change was found for positions 1927−1939 in the C-terminal part of the helix. These data correspond well with the intensity profile of cross-peaks in the HSQC NMR spectrum (Figure 4C) suggesting reduced mobility or exchange broadening in the C-terminal half of helix H3. A similar pattern is observed at the C-terminal part of helix H1. The high mobility at all positions apart from 1956 in helix 4, observed by EPR, and the absence of interhelical contacts indicate that the most likely reason for the reduced mobility in the C-terminal parts of helices H1 and H3 is the formation of transient helical structure in these regions, whose sequence favors helix formation. The existence of such structures would facilitate refolding of the bundle once vinculin is removed from the complex or may lead to helix repacking in the context of the whole talin rod. Very different characteristics were observed for helix H2, which becomes completely unstructured and highly mobile in the complex.

The indication from NMR and EPR that only one helix is immobilized in the complex agrees with the equimolar talin:Vd1 ratio in the complex. The consensus VBS sequence (*41*) agrees well with the experimental evidence that only helix H4 in the talin 1843−1973 bundle interacts with vinculin. Both the NMR and EPR data show clear evidence of an unfolding of the talin structure in the complex, with the sole exception of the VBS helix H4. This helix would be expected to be one of the most stable helices in the structure, since it contains a large number of bulky hydrophobic residues on its internal surface. In the context of the isolated talin 1843−1973 domain, the interaction of helix H4 with Vd1 led to total unfolding of the helical bundle, although this may be somewhat reduced in the whole talin rod, where the structure could potentially repack, establishing contacts between new sets of helices. As the binding surface is normally buried and inaccessible, the vinculin binding could be controlled through the stability of the domains containing the binding site, and indeed such a negative correlation between bundle stability and vinculin binding has been demonstrated through mutational analysis of the VBS2-containing domain (*56*). The exact mechanism of the conformational changes required for formation of the complex remains to be established. In particular, it is not clear whether the talin bundle unfolds to release the VBS which then binds to Vd1 or whether an interaction of Vd1 with the folded talin bundle promotes the unfolding of the latter; a detailed kinetic analysis will be needed to distinguish between these possibilities.

Despite the general similarities of the fold of talin 1843−1973 to helical bundles in other proteins, certain structural details emerge as unique features of the talin rod which are likely to be related to vinculin binding. The sequence of the talin rod has an unusually high alanine content. A high proportion of the alanine residues are involved in internal hydrophobic contacts, often arranged in clusters on the internal face of helices, making a continuous contact surface predominantly composed of alanine side chains. These clusters and the presence of some polar side chains on the inner surfaces of the helices reduce the area of hydrophobic contacts, leading to regions of decreased local stability. In both the VBS2-containing and VBS3-containing domains, side chains that are less than optimal for the packing of the hydrophobic core are concentrated in the second helix of the bundle. This helix in both cases contains a tyrosine residue that makes contacts with the hydrophobic core and appears to anchor the helix to the rest of the bundle. Thus, the emerging common characteristic of VBS-containing domains in the talin rod is a helical bundle arrangement with one of the helices having decreased stability and a smaller area of internal hydrophobic contact with the rest of the bundle. This creates a weak spot in the structure, allowing it to unfold when vinculin binds, providing access to the vinculin binding surface that is normally buried inside the bundle. The combined used of NMR and EPR proved to be a powerful approach to study the complex interaction between talin and vinculin, the two methods providing complementary data on the structure and dynamics of the complex and demonstrating clearly that the talin domain is largely unfolded in the complex. The folding of disordered proteins or protein domains on interaction with a partner has now been quite widely observed (e.g., ref *57*), but the phenomenon of "unfolding for binding" which has now been observed in all three of the talin rod domains studied to date (present work and refs *42* and *43*) is much less common. [An unfolding of the spectrin repeat of α-actinin to allow binding to vinculin has also been proposed (*58*), but as yet there is no direct experimental evidence for this.] This unfolding for binding suggests novel possibilities for regulation of the talin/vinculin interaction by modulation of the stability of the domains. For example, as noted above, in both the VBS2-containing and VBS3-containing domains a tyrosine residue on helix H2 appears to play an important role in stabilizing the hydrophobic core of the bundle, raising the possibility that they have a regulatory role through phosphorylation. We have recently shown that mutation of this key tyrosine in the 755−889 four-helix bundle to a glutamate results in a dramatic alteration in the conformation in the direction of unfolding, accompanied by an increased affinity for Vd1 (A. R. Gingras, B. Patel, J. Emsley, G. C. K. Roberts, D. R. Critchley, and I. L. Barsukov, unpublished work). This provides some support for the possibility that tyrosine phosphorylation would activate vinculin binding by talin, although it remains to be established whether this phosphorylation occurs in vivo.

NOTE ADDED AFTER ASAP PUBLICATION

This paper was published prematurely 01/20/06. Changes to the colors describing panel A of Figure 1 and panel C of Figure 3 were made, and the corrected version was published 01/20/06.

ACKNOWLEDGMENT

We thank Ronald Frank and Susanne Daenicke (GBF, Braunschweig) for synthesis of the SPOT-peptide array. We are grateful to Evangelos Papagrigoriou for many useful discussions.

SUPPORTING INFORMATION AVAILABLE

One table summarizing the experimental NMR restraints used for solving the solution structure of talin 1843−1973 and structural statistics and one figure showing analysis of Vd1 binding to a series of mouse VBS3 synthetic peptides (25-mers) in which ACM-Cys1953 was replaced by Ala, Ser, and 2-aminobutyric acid. This material is available free of charge via the Internet at http://pubs.acs.org.

REFERENCES

1. Critchley, D. R. (2004) Cytoskeletal proteins talin and vinculin in integrin-mediated adhesion, *Biochem. Soc. Trans. 32*, 831−836.
2. Calderwood, D. A., Zent, R., Grant, R., Rees, D. J., Hynes, R. O., and Ginsberg, M. H. (1999) The Talin head domain binds to integrin beta subunit cytoplasmic tails and regulates integrin activation, *J. Biol. Chem. 274*, 28071−28074.
3. Lee, H. S., Bellin, R. M., Walker, D. L., Patel, B., Powers, P., Liu, H., Garcia-Alvarez, B., de Pereda, J. M., Liddington, R. C., Volkmann, N., Hanein, D., Critchley, D. R., and Robson, R. M. (2004) Characterization of an actin-binding site within the talin FERM domain, *J. Mol. Biol. 343*, 771−784.
4. Garcia-Alvarez, B., de Pereda, J. M., Calderwood, D. A., Ulmer, T. S., Critchley, D., Campbell, I. D., Ginsberg, M. H., and Liddington, R. C. (2003) Structural determinants of integrin recognition by talin, *Mol. Cell 11*, 49−58.
5. Tadokoro, S., Shattil, S. J., Eto, K., Tai, V., Liddington, R. C., de Pereda, J. M., Ginsberg, M. H., and Calderwood, D. A. (2003) Talin binding to integrin beta tails: a final common step in integrin activation, *Science 302*, 103−106.
6. Kim, M., Carman, C. V., and Springer, T. A. (2003) Bidirectional transmembrane signaling by cytoplasmic domain separation in integrins, *Science 301*, 1720−1725.
7. Winkler, J., Lunsdorf, H., and Jockusch, B. M. (1997) Energy-filtered electron microscopy reveals that talin is a highly flexible protein composed of a series of globular domains, *Eur. J. Biochem. 243*, 430−436.
8. Xing, B., Jedsadayanmata, A., and Lam, S. C. (2001) Localization of an integrin binding site to the C terminus of talin, *J. Biol. Chem. 276*, 44373−44378.
9. Tremuth, L., Kreis, S., Melchior, C., Hoebeke, J., Ronde, P., Plancon, S., Takeda, K., and Kieffer, N. (2004) A fluorescence cell biology approach to map the second integrin-binding site of talin to a 130-amino acid sequence within the rod domain, *J. Biol. Chem. 279*, 22258−22266.
10. Hemmings, L., Rees, D. J., Ohanian, V., Bolton, S. J., Gilmore, A. P., Patel, B., Priddle, H., Trevithick, J. E., Hynes, R. O., and Critchley, D. R. (1996) Talin contains three actin-binding sites each of which is adjacent to a vinculin-binding site, *J. Cell Sci. 109*, 2715−2726.
11. McCann, R. O., and Craig, S. W. (1997) The I/LWEQ module: a conserved sequence that signifies F-actin binding in functionally diverse proteins from yeast to mammals, *Proc. Natl. Acad. Sci. U.S.A. 94*, 5679−5684.
12. Schmidt, J. M., Zhang, J., Lee, H. S., Stromer, M. H., and Robson, R. M. (1999) Interaction of talin with actin: sensitive modulation of filament cross-linking activity, *Arch. Biochem. Biophys. 366*, 139−150.
13. Isenberg, G., and Goldmann, W. H. (1998) Peptide-specific antibodies localize the major lipid binding sites of talin dimers to oppositely arranged N-terminal 47 kDa subdomains, *FEBS Lett. 426*, 165−170.
14. Chen, H. C., Appeddu, P. A., Parsons, J. T., Hildebrand, J. D., Schaller, M. D., and Guan, J. L. (1995) Interaction of focal adhesion kinase with cytoskeletal protein talin, *J. Biol. Chem. 270*, 16995−16999.
15. Borowsky, M. L. and Hynes, R. O. (1998) Layilin, a novel talin-binding transmembrane protein homologous with C-type lectins, is localized in membrane ruffles, *J. Cell Biol. 143*, 429−442.
16. Ling, K., Doughman, R. L., Firestone, A. J., Bunce, M. W., and Anderson, R. A. (2002) Type I gamma phosphatidylinositol phosphate kinase targets and regulates focal adhesions, *Nature 420*, 89−93.
17. Ling, K., Doughman, R. L., Iyer, V. V., Firestone, A. J., Bairstow, S. F., Mosher, D. F., Schaller, M. D., and Anderson, R. A. (2003) Tyrosine phosphorylation of type I gamma phosphatidylinositol phosphate kinase by Src regulates an integrin-talin switch, *J. Cell Biol. 163*, 1339−1349.
18. Di Paolo, G., Pellegrini, L., Letinic, K., Cestra, G., Zoncu, R., Voronov, S., Chang, S., Guo, J., Wenk, M. R., and De Camilli, P. (2002) Recruitment and regulation of phosphatidylinositol phosphate kinase type 1 gamma by the FERM domain of talin, *Nature 420*, 85−89.
19. Martel, V., Racaud-Sultan, C., Dupe, S., Marie, C., Paulhe, F., Galmiche, A., Block, M. R., and Albiges-Rizo, C. (2001) Conformation, localization, and integrin binding of talin depend on its interaction with phosphoinositides, *J. Biol. Chem. 276*, 21217−21227.
20. Seelig, A., Blatter, X. L., Frentzel, A., and Isenberg, G. (2000) Phospholipid binding of synthetic talin peptides provides evidence for an intrinsic membrane anchor of talin, *J. Biol. Chem. 275*, 17954−17961.
21. Jockusch, B. M., and Rudiger, M. (1996) Crosstalk between cell adhesion molecules: vinculin as a paradigm for regulation by conformation, *Trends Cell Biol. 6*, 311−315.
22. Demali, K. A. (2004) Vinculin−a dynamic regulator of cell adhesion, *Trends Biochem. Sci. 29*, 565−567.
23. Huttelmaier, S., Bubeck, P., Rudiger, M., and Jockusch, B. M. (1997) Characterization of two F-actin-binding and oligomerization sites in the cell-contact protein vinculin, *Eur. J. Biochem. 247*, 1136−1142.
24. Johnson, R. P., and Craig, S. W. (1995) F-actin binding site masked by the intramolecular association of vinculin head and tail domains, *Nature 373*, 261−264.
25. Johnson, R. P., and Craig, S. W. (2000) Actin activates a cryptic dimerization potential of the vinculin tail domain, *J. Biol. Chem. 275*, 95−105.
26. Johnson, R. P., and Craig, S. W. (1994) An intramolecular association between the head and tail domains of vinculin modulates talin binding, *J. Biol. Chem. 269*, 12611−12619.
27. Bakolitsa, C., Cohen, D. M., Bankston, L. A., Bobkov, A. A., Cadwell, G. W., Jennings, L., Critchley, D. R., Craig, S. W., and Liddington, R. C. (2004) Structural basis for vinculin activation at sites of cell adhesion, *Nature 430*, 583−586.
28. Borgon, R. A., Vonrhein, C., Bricogne, G., Bois, P. R., and Izard, T. (2004) Crystal structure of human vinculin, *Structure (Cambridge) 12*, 1189−1197.
29. Izard, T., Evans, G., Borgon, R. A., Rush, C. L., Bricogne, G., and Bois, P. R. (2004) Vinculin activation by talin through helical bundle conversion, *Nature 427*, 171−175.
30. Johnson, R. P., Niggli, V., Durrer, P., and Craig, S. W. (1998) A conserved motif in the tail domain of vinculin mediates association with and insertion into acidic phospholipid bilayers, *Biochemistry 37*, 10211−10222.
31. Bakolitsa, C., de Pereda, J. M., Bagshaw, C. R., Critchley, D. R., and Liddington, R. C. (1999) Crystal structure of the vinculin tail suggests a pathway for activation, *Cell 99*, 603−613.
32. Gilmore, A. P., and Burridge, K. (1996) Regulation of vinculin binding to talin and actin by phosphatidyl-inositol-4−5-bis-phosphate, *Nature 381*, 531−535.
33. Chandrasekar, I., Stradal, T. E., Holt, M. R., Entschladen, F., Jockusch, B. M., and Ziegler, W. H. (2005) Vinculin acts as a sensor in lipid regulation of adhesion-site turnover, *J. Cell Sci. 118*, 1461−1472.
34. Galbraith, C. G., Yamada, K. M., and Sheetz, M. P. (2002) The relationship between force and focal complex development, *J. Cell Biol. 159*, 695−705.

35. Coll, J. L., Ben-Ze'ev, A., Ezzell, R. M., Rodriguez Fernandez, J. L., Baribault, H., Oshima, R. G., and Adamson, E. D. (1995) Targeted disruption of vinculin genes in F9 and embryonic stem cells changes cell morphology, adhesion, and locomotion, *Proc. Natl. Acad. Sci. U.S.A. 92*, 9161−9165.
36. Xu, W., Coll, J. L., and Adamson, E. D. (1998) Rescue of the mutant phenotype by reexpression of full-length vinculin in null F9 cells; effects on cell locomotion by domain deleted vinculin, *J. Cell Sci. 111*, 1535−1544.
37. Xu, W., Baribault, H., and Adamson, E. D. (1998) Vinculin knockout results in heart and brain defects during embryonic development, *Development 125*, 327−337.
38. Gilmore, A. P., Wood, C., Ohanian, V., Jackson, P., Patel, B., Rees, D. J., Hynes, R. O., and Critchley, D. R. (1993) The cytoskeletal protein talin contains at least two distinct vinculin binding domains, *J. Cell Biol. 122*, 337−347.
39. Bass, M. D., Smith, B. J., Prigent, S. A., and Critchley, D. R. (1999) Talin contains three similar vinculin-binding sites predicted to form an amphipathic helix, *Biochem. J. 341*, 257−263.
40. McLachlan, A. D., Stewart, M., Hynes, R. O., and Rees, D. J. (1994) Analysis of repeated motifs in the talin rod, *J. Mol. Biol. 235*, 1278−1290.
41. Gingras, A. R., Ziegler, W. H., Frank, R., Barsukov, I. L., Roberts, G. C., Critchley, D. R., and Emsley, J. (2005) Mapping and consensus sequence identification for multiple vinculin binding sites within the talin rod, *J. Biol. Chem. 280*, 37217−37224.
42. Fillingham, I., Gingras, A. R., Papagrigoriou, E., Patel, B., Emsley, J., Critchley, D. R., Roberts, G. C., and Barsukov, I. L. (2005) A vinculin binding domain from the talin rod unfolds to form a complex with the vinculin head, *Structure (Cambridge) 13*, 65−74.
43. Papagrigoriou, E., Gingras, A. R., Barsukov, I. L., Bate, N., Fillingham, I. J., Patel, B., Frank, R., Ziegler, W. H., Roberts, G. C., Critchley, D. R., and Emsley, J. (2004) Activation of a vinculin-binding site in the talin rod involves rearrangement of a five-helix bundle, *EMBO J. 23*, 2942−2951.
44. Izard, T. and Vonrhein, C. (2004) Structural basis for amplifying vinculin activation by talin, *J. Biol. Chem. 279*, 27667−27678.
45. Delaglio, F., Grzesiek, S., Vuister, G. W., Zhu, G., Pfeifer, J., and Bax, A. (1995) NMRPipe: a multidimensional spectral processing system based on UNIX pipes, *J. Biomol. NMR 6*, 277−293.
46. Johnson, B. A., and Blevins, R. A. (1994) Software for the Visualization and Analysis of Nuclear Magnetic Resonance Data, *J. Biomol. NMR 4*, 603−614.
47. Sattler, M., Schleucher, J., and Griesinger, C. (1999) Heteronuclear multidimensional NMR experiments for the structure determination of proteins in solution employing pulsed field gradients, *Prog. NMR Spectrosc. 34*, 93−158.
48. Moseley, H. N., Monleon, D., and Montelione, G. T. (2001) Automatic determination of protein backbone resonance assignments from triple resonance nuclear magnetic resonance data, *Methods Enzymol. 339*, 91−108.
49. Herrmann, T., Guntert, P., and Wuthrich, K. (2002) Protein NMR structure determination with automated NOE assignment using the new software CANDID and the torsion angle dynamics algorithm DYANA, *J. Mol. Biol. 319*, 209−227.
50. Linge, J. P., O'Donoghue, S. I., and Nilges, M. (2001) Automated assignment of ambiguous nuclear overhauser effects with ARIA, *Methods Enzymol. 339*, 71−90.
51. McHaourab, H. S., Lietzow, M. A., Hideg, K., and Hubbell, W. L. (1996) Motion of spin-labeled side chains in T4 lysozyme. Correlation with protein structure and dynamics, *Biochemistry 3*, 7692−7704.
52. Steinhoff, H. J., Radzwill, N., Thevis, W., Lenz, V., Brandenburg, D., Antson, A., Dodson, G., and Wollmer, A. (1997) Determination of interspin distances between spin labels attached to insulin: comparison of electron paramagnetic resonance data with the X-ray structure, *Biophys. J. 73*, 3287−3298.
53. Frank, R., and Overwin, H. (1996) SPOT synthesis. Epitope analysis with arrays of synthetic peptides prepared on cellulose membranes, *Methods Mol. Biol. 66*, 149−169.
54. Hubbell, W. L., Cafiso, D. S., and Altenbach, C. (2000) Identifying conformational changes with site-directed spin labeling, *Nat. Struct. Biol. 7*, 735−739.
55. Hubbell, W. L., and Altenbach, C. (1994) Investigation of structure and dynamics in membrane proteins using site-directed spin labeling, *Curr. Opin. Struct. Biol. 4*, 566−573.
56. Patel, B. C., Gingras, A. R., Bobkov, A. A., Fujimoto, L. M., Zhang, M., Liddington, R. C., Mazzeo, D., Emsley, J., Roberts, G. C. K., Barsukov, I. L., and Critchley, D. R. (2005) The activity of the vinculin binding sites in talin is influenced by the stability of the helical bundles that make up the talin rod, *J. Biol. Chem.* (in press).
57. Wright, P. E., and Dyson, H. J. (1999) Intrinsically unstructured proteins: re-assessing the protein structure−function paradigm, *J. Mol. Biol. 29*, 321−331.
58. Bois, P. R., Borgon, R. A., Vonrhein, C., and Izard, T. (2005) Structural dynamics of alpha-actinin-vinculin interactions, *Mol. Cell. Biol. 25*, 6112−6122.

BI052136L